Deficiency of a sulfotransferase for sialic acid-modified glycans mitigates Alzheimer's pathology

Zui Zhang[a], Yoshiko Takeda-Uchimura[a], Tahmina Foyez[a], Shiori Ohtake-Niimi[a], Narentuya[a], Hiroyasu Akatsu[b,c], Kazuchika Nishitsuji[d], Makoto Michikawa[e,f], Tony Wyss-Coray[g], Kenji Kadomatsu[a], and Kenji Uchimura[a,f,1]

[a]Department of Biochemistry, Nagoya University Graduate School of Medicine, Nagoya, 466-8550, Japan; [b]Choju Medical Institute, Fukushimura Hospital, Toyohashi, 441-8124, Japan; [c]Department of Community-Based Medicine, Nagoya City University Graduate School of Medicine, Nagoya, 467-8601, Japan; [d]Department of Molecular Pathology, Tokushima University Graduate School of Biomedical Sciences, Tokushima, 770-8503, Japan; [e]Department of Biochemistry, Nagoya City University Graduate School of Medicine, Nagoya, 467-8601, Japan; [f]Department of Alzheimer's Disease Research, National Center for Geriatrics and Gerontology, Obu, 474-8511, Japan; and [g]Department of Neurology and Neurological Sciences, Stanford University School of Medicine, Stanford, CA 94305

Edited by Gabriel A. Rabinovich, University of Buenos Aires, Buenos Aires, Argentina, and approved February 23, 2017 (received for review September 9, 2016)

We previously showed that microglial keratan sulfate (KS) was induced in amyotrophic lateral sclerosis. However, the functional roles of the glycan and its synthetic enzyme in neurodegenerative diseases, such as Alzheimer's disease (AD), a progressive disorder, are unclear. In our study, KS modified with sialic acids having a molecular mass of 125–220 kDa and the carbohydrate sulfotransferase GlcNAc6ST1 were up-regulated in the brains of two transgenic mouse models (J20 and Tg2576) and the brains of patients with AD. GlcNAc6ST1-deficient J20 (J20/GlcNAc6ST1$^{-/-}$) mice demonstrated a complete absence of the microglial sialylated KS. J20/GlcNAc6ST1$^{-/-}$ primary microglia showed an increased level of amyloid-β phagocytosis and were hyperresponsive to interleukin 4, a potent antiinflammatory cytokine. Moreover, J20/GlcNAc6ST1$^{-/-}$ mice manifested reduced cerebral amyloid-β deposition. GlcNAc6ST1-synthesizing sialylated KS thus modulates AD pathology. Inhibition of KS synthesis by targeting GlcNAc6ST1 may therefore be beneficial for controlling AD pathogenesis.

Alzheimer's disease | carbohydrate-recognizing receptors | microglia | sialic acid | sulfotransferase

Cell-surface glycan structures are recognized by carbohydrate-binding receptors (lectins) (1, 2). These molecular recognitions govern cell–cell interactions in immune systems and tissue repair (3–5). Microglia are a type of myeloid cell population and are brain-resident immune cells (6–8). After microglia are stimulated, they manifest proinflammatory or antiinflammatory responses that are highly regulated by carbohydrate-binding receptors and their carbohydrate ligands (9, 10). Keratan sulfate (KS) is an extracellular glycan present in epithelial and neural tissues, including the brain. KS consists of repeating disaccharides of *N*-acetylglucosamine (GlcNAc) and galactose (Gal) with variable sulfate modifications at C-6 positions (11, 12). C-6 sulfation of KS is enzymatic, being catalyzed by GlcNAc/Gal/GalNAc sulfotransferases (13). KS sulfation and glycosyl modifications, e.g., sialylation, often change in response to injury or pathology (14, 15). GlcNAc6ST1, one of the sulfotransferases just mentioned, which was originally reported to be an L-selectin ligand enzyme (16), is expressed in the brain (17) and is required for microglial biosynthesis of highly sulfated sialylated epitopes of KS (18). The cell-surface 5D4-reactive KS has been suggested to have a role in microglial functions by binding via interactions with carbohydrate-binding receptors and molecules such as sialic acid-binding Ig-like lectins (siglecs) and galectins (10). By using the 5D4 monoclonal antibody (19), we found that the sialylated KS oligosaccharide structure, which has been reported in cartilage, was induced in microglia in a mouse model and in patients with amyotrophic lateral sclerosis (ALS) (18). The functional roles of the 5D4-reactive KS glycan and its synthetic enzyme in the pathogenesis of neurodegenerative diseases are unclear, however.

Alzheimer's disease (AD) is a progressive neurodegenerative disorder that is characterized by deposition of extracellular amyloid-β (Aβ) plaques and memory dysfunctions (20). Neuroinflammatory responses and neuronal toxicity of accumulated Aβ plaques are believed to contribute substantially to AD pathogenesis (21). Microglia play a vital role in immune regulation and homeostasis of the inflammatory environment in the vicinity of Aβ plaques in AD (22). Microglia directly phagocytose Aβ plaques and are indirectly involved in clearance of plaques as they release various cytokines (23). In our study here, we found that the 5D4-reactive KS glycan with a molecular mass of 125–220 kDa and GlcNAc6ST1 were up-regulated during disease progression in brains of AD mouse models and brains of patients with AD. The 5D4-reactive KS glycan was sialylated and expressed in microglia. We hypothesized that the sialylated 5D4-reactive KS may have a role in the regulation of microglial functions in AD pathogenesis. We successfully bred GlcNAc6ST1$^{-/-}$ mice (16) with J20 mice, a model of AD (24). GlcNAc6ST1-deficient J20 (J20/GlcNAc6ST1$^{-/-}$) AD model mice demonstrated a complete absence of microglial 5D4-KS. Primary microglia isolated from adult J20/GlcNAc6ST1$^{-/-}$ mice showed an increased level of Aβ phagocytosis and a hyperreactive response to interleukin 4 (IL-4), a potent antiinflammatory cytokine. Furthermore, J20/GlcNAc6ST1$^{-/-}$ mice had reduced levels of cerebral Aβ plaques. The processing of amyloid precursor protein was unchanged in the brains of J20/GlcNAc6ST1$^{-/-}$ mice. These results together indicate that GlcNAc6ST1 regulates microglial functions and that microglial 5D4-KS glycan may be a new therapeutic target in the AD brain via inhibiting the carbohydrate sulfotransferase.

Significance

Keratan sulfate (KS) is an extracellular sulfated glycan covalently attached to core proteins in the brain. Here, we show that a type of KS with a certain molecular mass in microglia and its synthetic enzyme GlcNAc6ST1, previously known as a sulfotransferase for ligands of L-selectin, are upregulated in model mice and patients with Alzheimer's disease. GlcNAc6ST1 deficiency resulted in increased amyloid-β phagocytosis and hyperresponsiveness to an antiinflammatory cytokine in primary microglia. Moreover, amyloid-β pathology was mitigated in GlcNAc6ST1-deficient Alzheimer's model mice. These data support a model in which GlcNAc6ST1 regulates microglial functions via synthesizing sialic acid-modified KS, a potential ligand for microglial carbohydrate-recognizing receptors, in Alzheimer's pathology.

Author contributions: K.U. designed research; Z.Z., Y.T.-U., T.F., S.O.-N., Narentuya, K.N., and K.U. performed research; H.A., M.M., T.W.-C., K.K., and K.U. contributed new reagents/analytic tools; H.A. contributed human specimens; Z.Z., Y.T.-U., S.O.-N., K.N., T.W.-C., and K.U. analyzed data; and Z.Z. and K.U. wrote the paper.

The authors declare no conflict of interest.

This article is a PNAS Direct Submission.

[1]To whom correspondence should be addressed. Email: arumihcu@med.nagoya-u.ac.jp.

This article contains supporting information online at www.pnas.org/lookup/suppl/doi:10.1073/pnas.1615036114/-/DCSupplemental.

Results

Sialylated 5D4-KS Expression Correlates with Aβ Pathogenesis in AD Mouse Models. We previously showed that expression of the 5D4-KS epitope was induced in ALS and that its expression increased with disease progression (18, 25). J20 and Tg2576 are AD transgenic mouse models that exhibit AD-like pathogenesis, including cerebral Aβ-plaque formation, synaptic loss, and gliosis with aging. To investigate expression of the 5D4-KS epitope in AD, we performed Western blotting with brain samples, which were prepared as Tris-buffered saline (TBS)-insoluble/1% SDS-soluble fractions, obtained from J20 and Tg2576 mice and their age-matched nontransgenic littermates. One major high-intensity band corresponding to 125–220 kDa was immunoreactive for 5D4 in cerebral samples from 20-mo-old J20 mice and 18-mo-old Tg2576 mice (Fig. 1*A* and *SI Appendix*, Fig. S1 *A* and *B*). Densitometric quantitative analysis of the intensities of the bands revealed 2.7- to 8-fold and 20-fold increases in cerebrum extracts of 20-mo-old J20 and 18-mo-old Tg2576 mice, respectively, compared with the increase in nontransgenic controls (Fig. 1*A* and *SI Appendix*, Fig. S1 *A* and *B*). A group of 6- to 8-mo-old J20 mice showed a 2.3-fold increase in the band intensities with a favorable trend ($P = 0.09$). A group of 2-mo-old J20 mice manifested comparable band intensities (Fig. 1*A*). We pretreated fractionated samples from 16-mo-old J20 mice with α2-3,6,8-neuraminidase (sialidase) or polysialic acid-cleaving endoneuraminidase N (Endo-N). We found a mobility shift of the major band (125–220 kDa) for the sialidase treatment but not for Endo-N, with the band being shifted to 115–170 kDa (Fig. 1*B*). These results clearly indicated that 5D4-KS was modified with mono- or oligosialic acids. The glycan was not modified with polysialic acids with a minimum length of 7–9 residues.

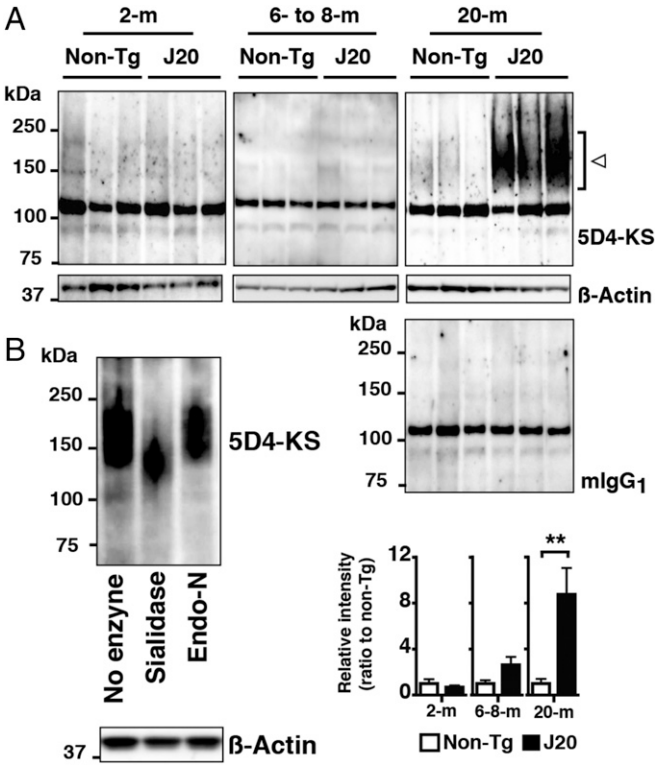

Fig. 1. Expression of sialylated 5D4-reactive KS is up-regulated in brains of aged J20 AD model mice. (*A*) TBS-insoluble/1% SDS-soluble fractions were prepared from homogenates of cerebral cortex obtained from 2- to 20-mo-old (2-m, 6- to 8-m, and 20-m) J20 mice. After Western blotting with 5D4 anti-KS antibody, densitometric quantitative analysis was used to measure intensities of bands with a molecular mass of 125–220 kDa (arrowhead). Bands of 120 kDa were also seen in isotype-matched control blots. $n = 3$ for nontransgenic controls (non-Tg) and $n = 3$ for J20 in each age group. (*B*) TBS-insoluble/1% SDS-soluble fractions of J20 hippocampal homogenates (16-mo-old mice) were pretreated with α2-3,6,8-neuraminidase (sialidase) or Endo-N at 37 °C overnight, followed by Western blotting with 5D4. β-Actin was used as a loading control. $^{**}P < 0.01$.

Microglial Localization of 5D4-KS in AD Model Mice. To determine which cells express 5D4-KS, we stained cryostat-cut brain sections from aged J20 mice with 5D4 and cell-type–specific markers (Fig. 2*A* and *SI Appendix*, Figs. S1*C* and S2). We found that 93–95% of the $5D4^+$ cells colocalized with signals of Iba1, a microglial marker, whereas signals of glial fibrillary acidic protein (GFAP), an astrocyte marker, did not colocalize with 5D4 signals in the hippocampus, cerebral cortex, and cerebellum (Fig. 2*A* and *SI Appendix*, Figs. S1*C*, S2, and S3). Signals of Ly6C, a marker of inflammatory monocytes, colocalized with 6% of the $5D4^+$ cells in the hippocampus but not in the cortex or cerebellum (*SI Appendix*, Figs. S2 *B* and *C* and S3). Of the $Iba1^+$ cells, 65% costained with 5D4 in the hippocampus (*SI Appendix*, Fig. S3). Triggering receptor expressed on myeloid cells 2 (TREM2) is a cell-surface receptor that is expressed in microglia and other myeloid cell populations of the central nervous system that regulates microglial phagocytosis and transmits intracellular signals that promote secretion of cytokines (26–28). To determine whether the 5D4 epitope is induced in $TREM2^+$ microglia, we stained J20 mouse brain sections with an anti-TREM2 antibody. TREM2 staining signals in the hippocampus were prominent in the soma, whereas 5D4-KS signals were seen in both the soma and microglial processes (Fig. 2*B* and *SI Appendix*, Fig. S4). About half the $5D4\text{-}KS^+$ microglia, which were identified by signals in the soma, costained with TREM2 signals in the J20 hippocampus (48%; *SI Appendix*, Fig. S4). Immunoelectron microscopy confirmed the signals seen in cell-surface membrane structures of microglia in the J20 hippocampus parenchyma (*SI Appendix*, Fig. S5). Iba1 expression is not restricted to microglia; other tissue-resident myeloid cells including vessel-associated myeloid types such as perivascular macrophages also express Iba1 (29). To see whether 5D4-KS was also expressed in vessel-associated myeloid cells, we used confocal microscopy of J20 mouse brain sections with an antibody against laminin, a marker of vascular basement membranes. We found that subsets of $5D4\text{-}KS^+$ cells were tightly associated with vessels (Fig. 2*C* and Movie S1). Immunoelectron microscopy revealed 5D4-KS signals in cell-surface membrane structures of vessel-associated myeloid cells and their processes (Fig. 2 *D*–*F*). Aβ-plaque–associated 5D4-KS signals were also detected in J20 and Tg2576 brains (*SI Appendix*, Fig. S6).

GlcNAc6ST1 Is the 5D4-KS Sulfotransferase and Regulates Microglial Aβ Phagocytosis and Cytokine Responses. We previously reported that GlcNAc6ST1 was up-regulated and mediated KS sulfation in vivo in ALS (18). To see whether GlcNAc6ST1 is also up-regulated during AD progression, we performed Western blotting with TBS-insoluble/1% SDS-soluble fractions prepared from brains of aged J20 and Tg2576 mice. Both J20 and Tg2576 mice demonstrated a significant increase in GlcNAc6ST1 protein level (1.7- to 2.2-fold increase) (Fig. 3*A* and *SI Appendix*, Fig. S7*A*). The expression level of the *Chst2* gene that encodes GlcNAc6ST1 was significantly up-regulated, whereas the other three genes encoding the murine GlcNAc6ST members, namely GlcNAc6ST2, GlcNAc6ST3, and GlcNAc6ST4, were unchanged in Tg2576 mice (*SI Appendix*, Fig. S7*B*). We then studied whether GlcNAc6ST1 is a synthetic enzyme of 5D4-KS induced in AD model microglial/myeloid cells. Clearly, brain sections prepared from aged $J20/GlcNAc6ST1^{-/-}$ mice did not have 5D4-KS staining signals (Fig. 3*B*), which confirmed that GlcNAc6ST1 is the carbohydrate sulfotransferase for the sialylated 5D4-KS glycan in the AD model brain. Western blotting showed a background level of the $5D4^+$ band signals in 20-mo-old $J20/GlcNAc6ST1^{-/-}$ mouse brains (*SI Appendix*, Fig. S8*A*).

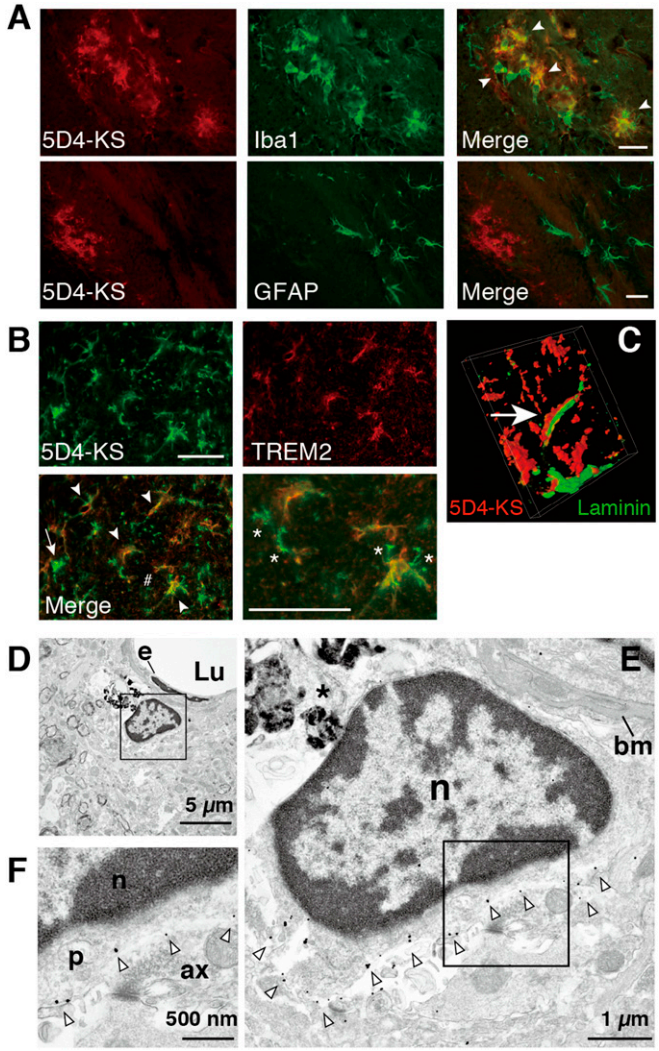

Fig. 2. Sialylated 5D4-reactive KS is expressed in microglia and vessel-associated myeloid cells in brains of aged J20 AD model mice. (*A*) Cryostat-cut sections of brains obtained from J20 mice were stained with 5D4 anti-KS (red) and an Iba1 microglial marker or an anti-GFAP astrocyte marker antibody (green). Arrowheads indicate 5D4-KS signals that colocalized with Iba1$^+$ microglial/myeloid cells. Representative hippocampus images are shown ($n = 3$, 18–20 mo old). (*B*) Cryostat-cut sections of brains from J20 mice were stained with 5D4 anti-KS (green) and TREM2, a microglial/myeloid cell marker (red). Representative hippocampus images are shown ($n = 3$, 24 mo old). Arrowheads indicate 5D4-KS signals that colocalized with TREM2. The arrow points to a 5D4-KS signal not colocalized with TREM2. In a high-magnification image of an area labeled with #, asterisks indicate representative 5D4$^+$ microglial processes. (Scale bars in *A and B*, 50 μm.) (*C*) Cryostat-cut section of brain from a J20 mouse was stained with 5D4 anti-KS (red) and an antibody against laminin, a marker of vasculature basement membrane (green). Representative Z-stack confocal microscopic image of the hippocampus is shown ($n = 3$, 18–24 mo old) (width, 109.81 μm; height, 109.81 μm; depth, 10 μm). The arrow points to 5D4-KS signals (red) associated with laminin signals (green) (Movie S1). (*D–F*) Representative preembedding immunoelectron microscopic images of 5D4-KS in a J20 hippocampus ($n = 2$, 18 mo old). Arrowheads in *E* point to gold-enhanced 5D4-KS signals along with membrane structures of the microglial cell surface and processes in the vessel abluminal area. The boxed area in *D* is magnified in *E*; that in *E* is magnified in *F*. A nuclear membrane lined with dense heterochromatin is a distinguishing feature of microglia. The asterisk in *E* indicates large inclusions of phagocytosed materials in the cytoplasm, which are common in these cells. Arrowheads in *F* mark 5D4-KS signals found in membrane structures in microglial cells in contact with an axon terminal. Lu, capillary lumen; e, endothelial cell; n, nucleus; bm, basement membrane; p, perikaryon; ax, axon terminal.

We assumed that the cell-surface 5D4-KS glycan may play a role in microglial Aβ phagocytosis and cell signaling on stimulation by binding through glycan-recognizing receptors. To test this hypothesis, we isolated CD11b$^+$ primary microglia from adult J20 and J20/GlcNAc6ST1$^{-/-}$ mice (Fig. 3*C*). Western blotting of cell extracts resulted in detection of the 5D4-reactive 125–220 kDa species in J20 primary microglia but not in microglia from J20/GlcNAc6ST1$^{-/-}$ mice (*SI Appendix*, Fig. S8*B*). We tested isolated CD11b$^+$ primary microglia for phagocytosis of fibril Aβ_{1-42} (fAβ_{1-42}). Both J20 and J20/GlcNAc6ST1$^{-/-}$ primary microglia internalized fAβ_{1-42}. One intriguing result was a significant increase (1.4-fold increase) in the number of phagocytic J20/GlcNAc6ST1$^{-/-}$ primary microglia (Fig. 3*D*). Quantification of internalized fAβ_{1-42} in fluorescence-positive individual cells showed an increased fAβ_{1-42} uptake (1.4-fold increase) in J20/GlcNAc6ST1$^{-/-}$ primary microglia (Fig. 3*D*). We then tested isolated primary microglia for a response to proinflammatory and antiinflammatory stimuli. As an interesting result, J20/GlcNAc6ST1$^{-/-}$ primary microglia showed a low response to a mixture of lipopolysaccharide (LPS) and IFN-γ proinflammatory agents, as shown by expression levels of their reactivating genes of tumor necrosis factor α (*Tnfα*) and IP-10 (*Cxcl10*) (Fig. 3*E*). J20/GlcNAc6ST1$^{-/-}$ primary microglia, however, manifested hyperreactivity to the antiinflammatory cytokine IL-4, as seen by levels of the responsive genes of arginase 1 (*Arg1*), macrophage mannose receptor (*Cd206*), and chitinase-like 3/Ym1 (*Chil3*) (Fig. 3*E*). Similar Aβ phagocytosis and response activities were observed in primary microglia isolated from adult GlcNAc6ST1$^{-/-}$ mice (*SI Appendix*, Fig. S9). These results motivated us to analyze the potential roles of GlcNAc6ST1 and the effects of microglial loss of the sialylated 5D4-KS on AD pathogenesis.

GlcNAc6ST1 Deficiency Attenuates Aβ Pathology. Cerebral deposition of Aβ plaques is a hallmark of AD pathology. In J20 mice, diffuse Aβ plaques reportedly started being deposited in the dentate gyrus and neocortex at 5–7 mo of age, and amyloid deposition was progressive, with widespread plaques occurring by 8–10 mo (24). Microglial activation contributed to some degree to a reduced Aβ plaque load in the AD model mice (30, 31). To discover whether GlcNAc6ST1 deletion would influence AD pathogenesis in vivo, we analyzed AD brain pathology of 9- to 15-mo-old J20/GlcNAc6ST1$^{-/-}$ mice. We found that Aβ deposition in the hippocampus was attenuated by 75% in J20/GlcNAc6ST1$^{-/-}$ mice compared with J20 littermates (Fig. 4*A*). In the J20/GlcNAc6ST1$^{-/-}$ hippocampus, Aβ-plaque loads in the molecular layer of the dentate gyrus were much less than those in the J20 hippocampus, whereas plaque loads near the hippocampal fissure were comparable (Fig. 4*A*). An increased number of reactive astrocytes near Aβ plaques, as revealed by detection of GFAP, is a feature of neuronal inflammation that correlates with microglial activation (32). We assessed anti-GFAP staining signals in J20/GlcNAc6ST1$^{-/-}$ mice. GFAP signals increased 1.8-fold in J20 mice, whereas the level of GFAP signals in the J20/GlcNAc6ST1$^{-/-}$ hippocampus was higher, but not significantly so, compared with the wild-type (WT) level (Fig. 4*A*). Synaptic loss is another characteristic of J20 AD model mice. In J20/GlcNAc6ST1$^{-/-}$ mice, a reduction in staining signals by an antibody against synaptophysin, a presynaptic marker, was moderate and not significantly different from the WT level (Fig. 4*A*). Of note, GlcNAc6ST1$^{-/-}$ mice showed a slight increase (1.2-fold) in synaptophysin signals compared with WT mice. Immunoreactivities of an antibody against NeuN, a neuronal marker, were comparable in all genotypes, which confirmed that neither J20 transgene expression nor GlcNAc6ST1 deficiency resulted in neuronal loss (*SI Appendix*, Fig. S10). To gain more insight into the possible effects of GlcNAc6ST1 deficiency on brain functions, especially blood–brain barrier (BBB) function, we used an in vivo Evans blue dye assay with GlcNAc6ST1$^{-/-}$ mice to

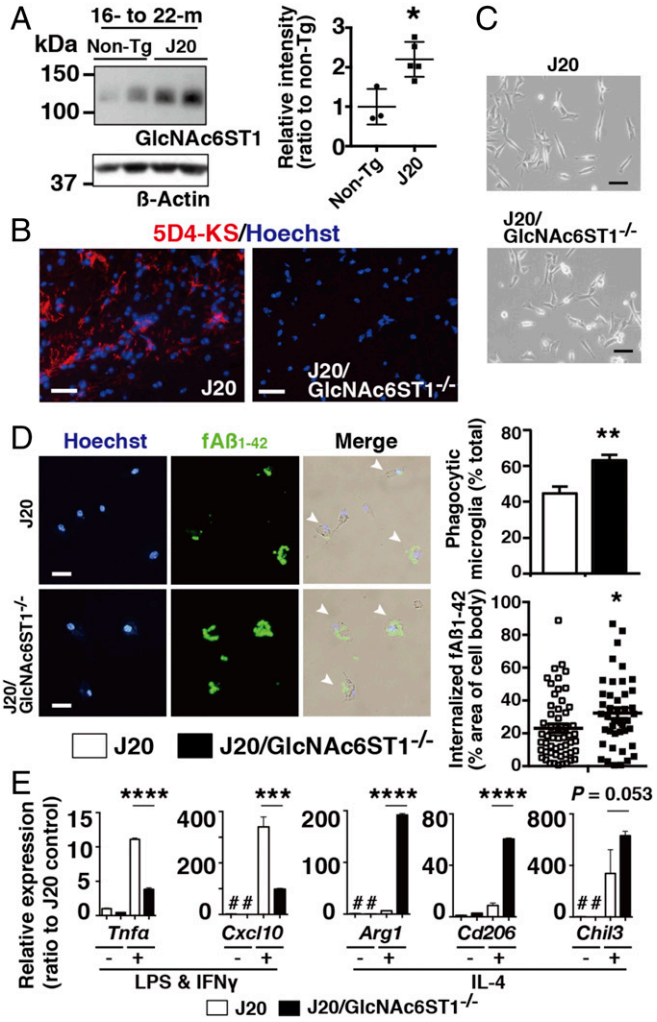

Fig. 3. Deficiency of the 5D4-KS sulfotransferase GlcNAc6ST1 leads to increased phagocytosis of $fA\beta_{1-42}$ and an altered response to cytokines in primary microglia. (*A*) TBS-insoluble/1% SDS-soluble fractions were prepared from homogenates of hippocampus obtained from 16- to 22-mo-old J20 mice and non-Tg littermates ($n = 3$ for non-Tg; $n = 5$ for J20). The average ages of the groups were 20 mo old (non-Tg) and 18 mo old (J20). After Western blotting with an anti-GlcNAc6ST1 antibody, densitometric quantitative analysis measured intensities of the bands. $^*P < 0.05$. (*B*) Cryostat-cut sections of brains from J20 and J20/GlcNAc6ST1$^{-/-}$ mice were stained with 5D4 anti-KS antibody (red) ($n = 3$ for each genotype, 18–24 mo old). The average ages of the groups were 21 mo old (J20) and 18 mo old (J20/GlcNAc6ST1$^{-/-}$). Hoechst was used to stain nuclei (blue). Representative hippocampal signals are shown. (Scale bars, 50 μm.) (*C*) Primary microglia were isolated from 2- to 6-mo-old J20 and J20/GlcNAc6ST1$^{-/-}$ mice ($n = 3$; average age for each genotype: 4 mo old) with a MACS microglial isolation kit (Miltenyi Biotec). CD11b bead-bound microglia were cultured for 14 d. Representative phase-contrast photomicrographs of isolated cells are shown. (Scale bars, 50 μm.) (*D*) Cultured microglia were incubated with $fA\beta_{1-42}$ (0.5 μM) for 24 h, fixed with 2% (wt/vol) PFA, and then stained with 82E1 anti-Aβ (green) and Hoechst (blue). Representative images of overlays of phase-contrast and fluorescence-staining signals are shown. The numbers of phagocytic cells (arrowheads) were quantitated. The $fA\beta_{1-42}$ signal intensity in individual cells was measured. Each dot represents one cell. Data are means ± SEM. (Scale bars, 25 μm.) $^*P < 0.05$, $^{**}P < 0.01$. (*E*) Primary microglia were stimulated with a mixture of LPS and IFN-γ or IL-4 for 24 h ($n = 3$ for each genotype). Levels of mRNA expression of their responsive genes with or without the stimulation were determined by quantitative real-time PCR. Columns with mean values of ≤1 are identified with #. $^{***}P < 0.001$, $^{****}P < 0.0001$.

measure the integrity of the BBB (33). GlcNAc6ST1$^{-/-}$ mice showed comparable leakage of Evans blue dye in the cerebrum and cerebellum under physiological and hyperosmolar conditions (*SI Appendix*, Fig. S11). BBB integrity was thus unaltered by GlcNAc6ST1 deficiency. The possibility existed that GlcNAc6ST1 deletion would have a positive impact on expression of the J20 transgene and lead to an increased level of the full-length

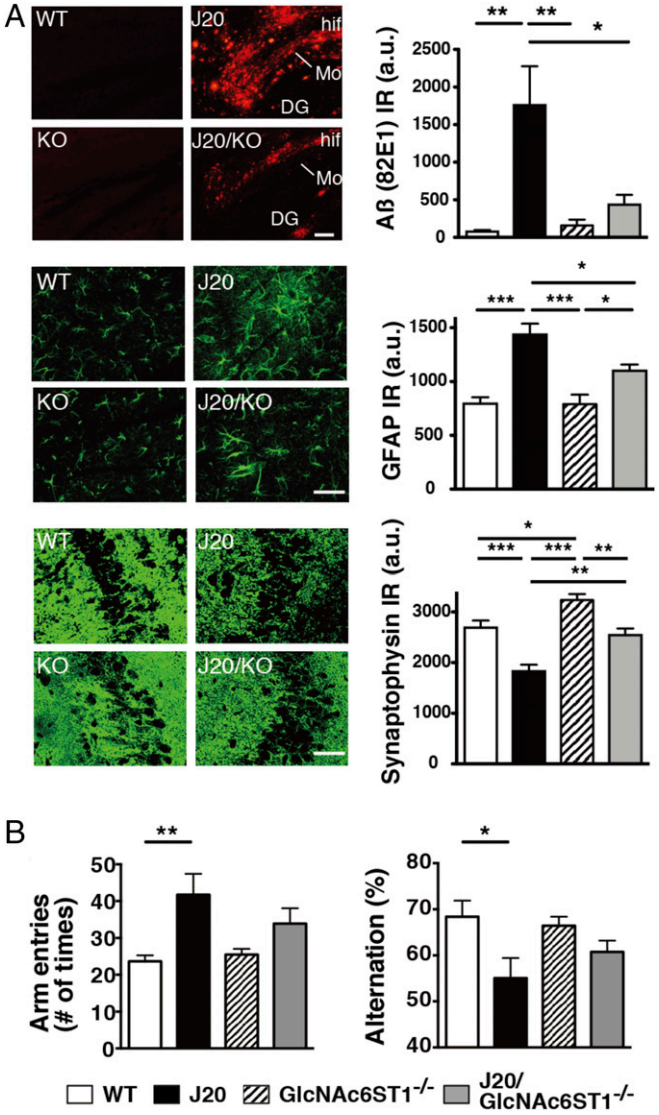

Fig. 4. GlcNAc6ST1 deficiency attenuates Aβ pathogenesis in J20 AD model mice. (*A*) Cryostat-cut sections of brains obtained from 9- to 15-mo-old mice were stained with 82E1 anti-Aβ (red), an anti-GFAP astrocyte marker antibody (green), or an antisynaptophysin presynaptic marker (green). $n = 6$ for WT, J20, GlcNAc6ST1$^{-/-}$ (knockout, KO), and J20/GlcNAc6ST1$^{-/-}$ (J20/KO) mice. The average ages of the groups were 13 mo old (WT), 14 mo old (J20), 13 mo old (KO), and 11 mo old (J20/KO). Levels of Aβ deposition, astroglial activation, and a presynaptic protein were determined by using the percent area of the immunoreactivity (IR) of 82E1, anti-GFAP, and anti-synaptophysin, respectively. Signals of representative hippocampus images are shown. The synaptophysin IR in the CA3 region was determined. hif, hippocampal fissure; Mo, molecular dentate gyrus layer; DG, dentate gyrus; a.u., arbitrary unit. $^*P < 0.05$, $^{**}P < 0.01$, $^{***}P < 0.001$. [Scale bars, (*Top*) 100 μm; (*Middle* and *Bottom*) 50 μm.] (*B*) Spontaneous alternation behavior in the Y maze was evaluated with 9- to 15-mo-old WT ($n = 9$), J20 ($n = 8$), GlcNAc6ST1$^{-/-}$ ($n = 11$), and J20/GlcNAc6ST1$^{-/-}$ ($n = 12$) mice. The average ages of the groups were 13 mo old (WT), 13 mo old (J20), 12 mo old (GlcNAc6ST1$^{-/-}$), and 11 mo old (J20/GlcNAc6ST1$^{-/-}$). J20 mice manifested a significant reduction in alternation and a significant increase in the number of arm entries, whereas those measures in J20/GlcNAc6ST1$^{-/-}$ mice were not significantly different from the WT levels. $^*P < 0.05$, $^{**}P < 0.01$.

amyloid precursor protein (FL-APP) and the β C-terminal fragment (β-CTF) that is generated by subsequent β-secretase cleavage of APP. Samples of TBS-insoluble/1% SDS-soluble fractions of J20 and J20/GlcNAc6ST1$^{-/-}$ mouse brains were subjected to immunoblotting with anti-APP (N) antibody or anti-APP (C) antibody. We found comparable levels of FL-APP and α/β-CTF (*SI Appendix*, Fig. S12*A*). Soluble sAPPα/β levels in TBS-soluble fractions were also measured via immunoblotting, and signals showed no significant difference in J20/GlcNAc6ST1$^{-/-}$ mice (*SI Appendix*, Fig. S12*A*). The mRNA levels of the human APP transgene and of the genes *Bace1* and *Psen1* in J20/GlcNAc6ST1$^{-/-}$ mouse brains were comparable to those in J20 mice (*SI Appendix*, Fig. S12*B*). Thus, GlcNAc6ST1 deletion reduced the Aβ-plaque load but did not affect processing of the transgene product APP. An interesting finding was the significantly up-regulated mRNA expression of neprilysin and insulin-degrading enzyme genes in J20/GlcNAc6ST1$^{-/-}$ mouse brains (*SI Appendix*, Fig. S13*A*). Expression levels of the genes *Cd115*, *Ly6c*, and *Ccr2* as inflammatory monocyte markers were unchanged. The IL-4 mRNA level was significantly up-regulated and IGF1 tended to increase in J20/GlcNAc6ST1$^{-/-}$ mouse brains (*SI Appendix*, Fig. S13 *B* and *C*).

Because AD brain pathogenesis causes memory deficits, we asked whether reduced Aβ-plaque deposition in J20/GlcNAc6ST1$^{-/-}$ mice would correlate with attenuation in memory impairment. To address this issue, we evaluated spontaneous alternation behaviors by testing the performance of all genotypes at 9–15 mo old in the Y maze. J20 mice showed a significant reduction in alternation and an increase in the number of arm entries, whereas these measures in J20/GlcNAc6ST1$^{-/-}$ mice were not significantly different from those for WT mice (Fig. 4*B*).

5D4-KS with a Molecular Mass of 125–190 kDa and GlcNAc6ST1 Are Up-Regulated in the Brains of Patients with AD. We also asked whether patients with AD would manifest the expression of 5D4-KS observed in J20 and Tg2576 AD model mice. We first performed Western blotting with postmortem hippocampus samples obtained from nondemented controls (NDCs) and patients with sporadic AD (*SI Appendix*, Table S1). Unlike the situation in the mouse brain, in which cerebral 5D4-reactive bands of >460 kDa occur at an early postnatal stage but not in adulthood (34), NDC samples showed 5D4-immunoreactive bands with sizes of >460 kDa (Fig. 5*A*). The intensities of these bands were reduced in AD, and 5D4-immunoreactive bands of 125–190 kDa, which are similar to 5D4 bands seen in J20 and Tg2576 AD model mice, also appeared (Fig. 5*A*).

Lindahl et al. previously reported that the total amounts of KS in the cerebral cortex of patients with AD were reduced to less than 50% of control values (35). We investigated whether the total KS amount would be altered in the hippocampus of patients with AD. Frozen postmortem brain samples were subjected to reversed-phase ion-pair HPLC, which we also used for another class of sulfated glycans (36). With regard to the KS amount and disaccharide compositions, the total amount of KS in the AD hippocampus was reduced to 43% of NDC values (Fig. 5*B*). The fractions of the monosulfated disaccharide unit, Galβ1–4GlcNAc(6S), and the disulfated disaccharide unit, Gal(6S)β1–4GlcNAc(6S), from the AD hippocampus were comparable to those of NDCs (*SI Appendix*, Fig. S14*A*), which indicated that synthesis of both Galβ1–4GlcNAc(6S) and Gal(6S)β1–4GlcNAc(6S) was reduced in AD. Immunohisotochemical staining showed predominant 5D4 staining signals in the neuropil of postmortem hippocampus specimens from NDCs, whereas these signals were greatly reduced in patients with AD (*SI Appendix*, Fig. S14*B*). Signals with a conspicuous process-like pattern were observed for 5D4 in AD (*SI Appendix*, Fig. S14*B*). Consistent with the result for the J20 and Tg2576 AD mouse models, a 3.3-fold increase in the expression of GlcNAc6ST1 was observed in the AD hippocampus postmortem (Fig. 5*C*).

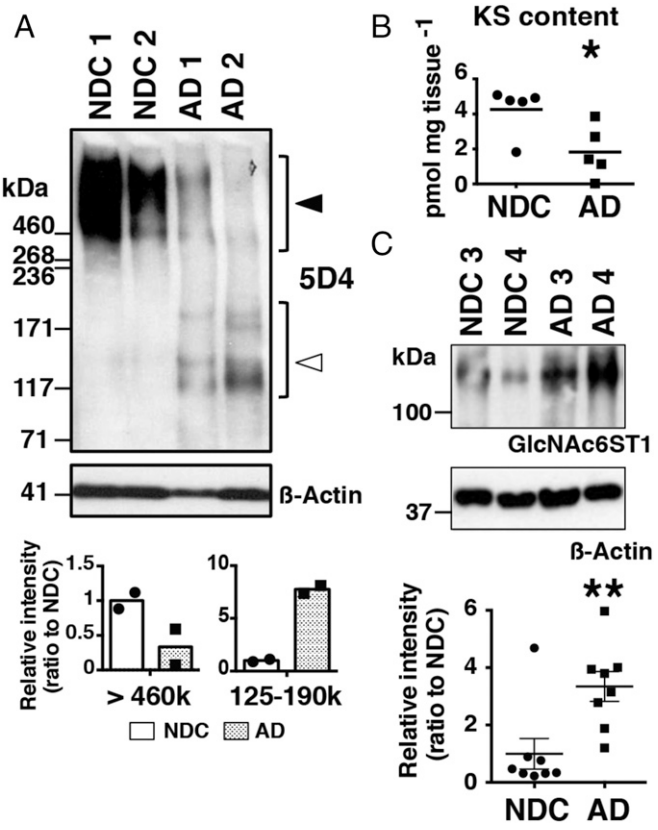

Fig. 5. 5D4-KS with a molecular mass of 125–190 kDa and GlcNAc6ST1 are up-regulated in patients with AD postmortem. (*A*) TBS-insoluble/1% SDS-soluble fractions were prepared from homogenates of hippocampus obtained postmortem from patients with NDCs and AD. After Western blotting with 5D4 antibody (n = 2 for each group), densitometric quantitative analysis was used to measure intensities of the bands with a molecular mass of >460 kDa (solid arrowhead) and 125–190 kDa (open arrowhead). (*B*) KS glycosaminoglycans were purified from homogenates of hippocampus obtained postmortem from NDCs (n = 5) and patients with AD (n = 5). Total KS content was measured via reversed-phase ion-pair HPLC combined with a system of postcolumn fluorescent labeling (36). *P < 0.05. (*C*) Western blotting was performed with anti-GlcNAc6ST1 antibody (n = 8 for each group). Representative results are shown (n = 2 for each group). Densitometric quantitative analysis was used to measure intensities of the bands. β-Actin was used as a loading control. **P < 0.01.

Discussion

We show here that microglial 5D4-KS is a sialic acid-modified glycan with a precise molecular mass and that glycans are induced in parallel with the increased GlcNAc6ST1 protein by AD progression in AD mouse models and patients with AD. GlcNAc6ST1 deficiency results in glycan depletion, increased fibrillar Aβ phagocytosis, and a hyperresponsiveness to the potent antiinflammatory cytokine IL-4 in microglia. Moreover, genetic loss of the sulfotransferase resulted in a great reduction of Aβ-plaque deposition in an AD mouse model. These findings establish an adverse effect of microglial GlcNAc6ST1 on AD pathogenesis.

Our previous study with model mice and patients with ALS indicated that microglial 5D4-KS was sialylated (18). These glycans are short mucin-type glycans with a probable structure of Siaα2–3Gal(6S)β1–4GlcNAc(6S)β1–3Galβ1–4(α1–3Fuc)GlcNAc(6S)β1–6R or –2R (R indicates GalNAc or mannose). Siglecs are cell-surface transmembrane molecules that comprise a family of carbohydrate-binding receptors expressed on circulating and tissue-resident leukocytes including microglia, and they regulate immune function (5, 37). All siglecs recognize glycans with sialic acid termini that have *cis* (ligands on the same cell) or *trans* (ligands on other cells) functions.

A group of CD33-related siglecs preferentially bound to sialylated, sulfated glycans that were composed of Gal(6S) or GlcNAc(6S) (37–40). Because microglial 5D4-KS was extracted in TBS-insoluble/1% SDS-soluble fractions, molecules modified with 5D4-KS are conceivably cell-surface membrane proteins. Although the roles of the sialyl 5D4-KS are still not clear, glycans may work as *cis* ligands for siglecs expressed in microglia (41, 42) and may regulate molecular clustering of carbohydrate-binding receptors within cell-surface membranes, thereby modulating microglial cell signaling. Identification of 5D4-KS core proteins and signaling pathways is needed to clarify whether the binding receptors are stimulatory or inhibitory.

Sialylated 5D4-KS was expressed in surface membrane structures of cells positive for Iba1, a marker of microglial and other myeloid cell populations in the brain (29). That a subset of 5D4-KS$^+$ cells may include inflammatory monocytes is conceivable because a small proportion of 5D4-KS$^+$ cells colocalized with signals of Ly6C. To confirm this result, additional analyses with antibodies against other inflammatory monocyte markers such as CCR2 are needed. Here, 5D4-KS$^+$ cells were associated with Aβ plaques in J20 and Tg2576 AD mouse brains. Considerable evidence has demonstrated that activated microglia cluster at sites of aggregated Aβ plaques and contribute to Aβ clearance in the early phases of neurodegeneration (43, 44). TREM2 is expressed in microglia in the brain, and its rare mutation is a risk factor for late-onset AD (45). TREM2$^+$ microglia accumulate around Aβ plaques. AD model mice deficient in TREM2 have shown a reduction in Aβ-plaque–associating microglial/myeloid cells (27, 28) and age-dependent amelioration of amyloid pathology (28, 44). In this study here, we found that about 50% of cells expressing 5D4-KS were TREM2$^+$. To some extent, 5D4-KS may have a role that may correlate with that of TREM2, as seen in J20/GlcNAc6ST1$^{-/-}$ mice, which manifested amelioration of AD pathogenesis. As an interesting result, 5D4-KS was also expressed in vessel-associated microglial/myeloid cells. Iba1$^+$ myeloid cell populations are heterogeneous and have diverse roles in AD pathology (29). 5D4-KS may be expressed in perivascular macrophages, which are almost indistinguishable from microglial cells and contribute to clearance of Aβ. By using genetic ablation systems in which peripherally derived myeloid cells are recruited and replaced with microglia in the AD brain, we may address the question of whether a subset of 5D4-KS cells resides in the brain (46, 47).

The GlcNAc6ST1 gene *Chst2* was identified as one of the 40 most differentially expressed genes in microglia during ALS disease progression (48). In the present study, we found that cerebral GlcNAc6ST1 was up-regulated both in aged AD model mice and in patients with AD postmortem. Microglia produce sialylated 5D4-KS in a GlcNAc6ST1-dependent manner during AD progression, as in ALS pathogenesis (18). That GlcNAc6ST1 is induced by Aβ pathology in microglia during AD progression is strongly suggested. Our genetic ablation study indicated that GlcNAc6ST1 was required for synthesis of the microglial sialyl 5D4-KS glycan and that loss of the carbohydrate sulfotransferase increased the number of phagocytic microglia for fAβ_{1-42}. Promotion of phagocytosis in microglia correlates with a reduction in insoluble Aβ42 level and Aβ-plaque load in AD brain as shown by inactivation of the siglec CD33 (42). It is plausible that the sialylated 5D4-KS could be recognized by CD33 in a *cis*-acting manner and involved in Aβ phagocytosis. Pretreatment of microglia with bacterial keratan sulfate endo-1,4-β-galactosidase in conjunction with sialidases would be a useful approach to analyze these possibilities (18). GlcNAc6ST1 deficiency also showed an altered microglial response to IL-4 as cells became hyperreactive to it. Alternatively, activated microglia reportedly showed neuroprotective effects in neurodegenerative diseases (32). Reduced Aβ-plaque loads in J20/GlcNAc6ST1$^{-/-}$ mice may be explained in part by the possibility that GlcNAc6ST1 deficiency in microglia has a protective role in AD pathogenesis by promoting Aβ clearance with phagocytosis and altering inflammation near Aβ plaques. Determination of the amyloid plaque load with thioflavin S or methoxy-X04 would aid our understanding of mechanisms underlying amyloidosis and Aβ-plaque pathology in J20/GlcNAc6ST1$^{-/-}$ brains. Reduced level of astrogliosis observed in J20/GlcNAc6ST1$^{-/-}$ mice may be attributable to altered astrocyte reactivation by cytokines and chemokines secreted from differentially activated microglia around Aβ plaques (23, 32). Perhaps, synaptic loss mediated by microglia could be attenuated to some extent by GlcNAc6ST1 deficiency. Clarifying the up-regulated mRNA levels of the genes encoding neprilysin, insulin-degrading enzyme, and IL-4 in the J20/GlcNAc6ST1$^{-/-}$ hippocampus would be an intriguing topic for future studies. Although the measures of spontaneous alternation behavior approached WT levels in J20/GlcNAc6ST1$^{-/-}$ mice, these values did not differ statistically from those in J20 mice revealed by Tukey's multiple comparison test (P = 0.42 in the arm entry, P = 0.55 in the alternation behavior). To address the question of whether GlcNAc6ST1 deficiency induces attenuation of memory impairment, other behavioral tests such as the Morris water maze test and the novel object recognition test should be performed with J20/GlcNAc6ST1$^{-/-}$ mice. Additional study is required to clarify the mechanisms underlying the alleviation of AD pathogenesis.

Although we found that 5D4-KS was selectively induced in the AD mouse model brain, one report described selective loss of the total amount of KS in the brain of patients with AD (35). To explain this discrepancy, we analyzed brains of patients with AD by quantification of the KS structure. We previously analyzed the total amounts of heparan sulfate, another class of glycosaminoglycan, in brains of patients with AD (36). Here, we used the same analytical method for KS. Although we could not perform an analysis of KS structure by using this method with adult mouse brains for an unknown reason, we succeeded in analyzing postmortem human brain samples. The hippocampus of patients with AD showed a significantly reduced total amount of KS and decreased 5D4 immunoreactivity in the neuropil. These results are consistent with the above-mentioned report that overall KS in the cerebral cortex was reduced in postmortem brains of patients with AD (35). We assessed the brains of patients with AD by immunoblotting with 5D4. Adult mouse brains had a negligible level of 5D4-KS without the neurodegeneration seen in our present study and our previous study (34). A surprising result was that 5D4-KS glycan-carrying molecules were apparently present in human control brains (NDCs) as a high-molecular-mass form (>460 kDa). These high-molecular-mass species were dramatically reduced in AD, with a concomitant appearance of bands of smaller size (125–190 kDa), which were similar to bands in the AD model mice. This result strongly suggests that the total amount of KS in the human brain detected by these analytical methods would largely account for the expression of the 5D4-KS$^+$ >460 kDa molecules rather than the 125- to 190-kDa species. The >460-kDa 5D4-KS glycans may be formed of expanded repeat units of C6-sulfated Galβ1–4GlcNAc synthesized by other members of GlcNAc6ST in neurons. One candidate core protein of the >460-kDa 5D4-KS glycans in human brains may be phosphacan; we previously showed that the 5D4 epitope is present in early postnatal brains in mice (34). Identification of core proteins for the >460-kDa and 125- to 190-kDa species would promote a better understanding of which cell types produce these species and what molecular mechanisms underlie microglial activation and neurodegeneration. Thus, our structural analysis with human AD brains clearly indicates that total amounts of KS were reduced but that 5D4-KS signals with the size 125–190 kDa occurred during AD pathogenesis in patients. We therefore propose that inhibition of 5D4-KS synthesis in microglia by targeting GlcNAc6ST1 may be a beneficial approach to ameliorate AD pathogenesis.

Materials and Methods

Materials. Materials were obtained from the commercial sources indicated as follows: 5D4 anti-keratan sulfate (anti-KS) monoclonal antibody was from Cosmo Bio; rabbit anti-GlcNAc6ST1/CHST2 antibody was from Sigma; sheep anti-TREM2 antibody was from R&D Systems; mouse anti-amyloid β (anti-Aβ) (N terminus) (82E1) antibody was from IBL; rabbit anti-GFAP antibody was from Thermo Fisher Scientific; rabbit anti-Iba I antibody was from Wako; rabbit anti-synaptophysin was from Frontier Institute; rabbit anti-laminin antibody and LPS (from *Escherichia coli* 0111:B4) were from Sigma; murine IFN-γ and IL-4 were from PeproTech; α2-3,6,8-neuraminidase (sialidase, *Arthrobacter ureafaciens*) was from Nacalai Tesque; and Endo-N (phage K1) was from AbCys.

Mice. J20 transgenic mice (24) that expressed human APP (hAPP) bearing Swedish (K670N/M671L) and Indiana (V717F) mutations were obtained from The Jackson Laboratory. Tg2576 transgenic mice (49) with the hAPP Swedish (K670N/M671L) mutation were purchased from Taconic. The generation of GlcNAc6ST1-deficient (GlcNAc6ST1$^{-/-}$) mice was described previously (50). All experimental procedures were approved by the Animal Research Committee of Nagoya University and National Center for Geriatrics and Gerontology and were conducted according to guidelines of Nagoya University and National Center for Geriatrics and Gerontology.

Postmortem Human Brain Tissues. Each patient with sporadic AD had a pathological diagnosis determined according to criteria of the Consortium to Establish a Registry for Alzheimer's Disease and the Braak stage. Elderly age-matched patients without significant neurological disorders were placed into an NDC group. AD diagnoses were confirmed by using clinical and pathological criteria (*SI Appendix*, Table S1). The written informed consent was obtained from all human subjects. Further details on postmortem tissues are supplied in *SI Appendix, SI Materials and Methods*.

Isolation of Primary Microglial Cells from Adult Mice. Microglial cells were prepared as previously described (18). We used the method of Hickman et al. (51) with a slight modification. More details on primary microglial assays are supplied in *SI Appendix, SI Materials and Methods*.

Western Blotting and Densitometry. TBS-insoluble/1% SDS-soluble fractions (40 μg of protein per lane) were separated via NuPAGE 3–8% polyacrylamide gel electrophoresis (Thermo Fisher Scientific) and blotted onto polyvinylidene difluoride membranes. The blots were probed with primary antibodies at 4 °C overnight after blocking with 5% (wt/vol) skim milk/PBS containing 0.1% Tween-20 for 1 h at room temperature. The immunoreactive bands were visualized with horseradish peroxidase-conjugated secondary antibodies followed by using an ECL-Plus Western Blotting Detection Kit (GE Healthcare) and autoradiography. Densitometric analysis of immunoreactive bands was performed on a Macintosh computer with the use of the ImageJ software version 1.44 (NIH; imagej.nih.gov/ij/). Levels of 5D4-KS and GlcNAc6ST1 were normalized to the levels of β-actin to control for protein loading. For enzymatic treatment, TBS-insoluble/1% SDS-soluble fractions (60 μg of protein per reaction) were digested with sialidase (0.1 U·mL^{-1}) or Endo-N (58 U·mL^{-1}) at 37 °C overnight. Enzymatic reactions were stopped by heating the samples at 95 °C for 5 min.

fAβ$_{1-42}$ Phagocytosis Assay. Aβ peptide (human, 1–42) (Peptide Institute) was dissolved in 0.1% NH_3 in a 1-mM stock solution. After dilution in PBS to 100 μM, the Aβ$_{1-42}$ solution was incubated at 37 °C for 5 d to prepare fAβ$_{1-42}$. Primary microglia were isolated from WT, GlcNAc6ST1$^{-/-}$, J20, and J20/GlcNAc6ST1$^{-/-}$ mice (2–6 mo old) by using CD11b magnetic beads as described above. Isolated microglia were cultured with 0.5 μM fAβ$_{1-42}$ in Opti-MEM (Thermo Fisher Scientific) for 24 h at 37 °C in cultured glass slides (BD Biosciences). After cells were washed in PBS, they were fixed in 2% (wt/vol) paraformaldehyde (PFA) for 1 h and then incubated with 3% (wt/vol) BSA for 1 h at room temperature for blocking. The fAβ$_{1-42}$ uptake signal was detected with biotinylated 82E1 antibody (1:100) followed by Cy2-labeled streptavidin (1:250). Digital images of five randomly selected fields in the cultured glass slides were captured. The number of phagocytic cells was counted and quantitated as a percentage of total cells in each field.

Immunohistochemistry. Frozen mouse brain tissues were cut into 10-μm-thick sections via a cryostat and collected on MAS-coated glass slides (SF17293; Matsunami). Sections were air dried for 30 min, rinsed with PBS to remove optimal cutting temperature compound, and blocked in 3% (wt/vol) BSA in PBS for 1 h at room temperature. Sections were then incubated overnight at 4 °C with a mixture of biotinylated 82E1 (1:50 dilution) and rabbit anti-GFAP, rabbit anti-Iba1, or rabbit anti-laminin antibody (1:100 dilution; Sigma) in 0.1% BSA in PBS. After the samples were washed in PBS, primary antibodies were detected with Cy3-conjugated streptavidin (6.8 μg·mL^{-1}; Jackson ImmunoResearch) and Alex-488–conjugated polyclonal goat anti-rabbit IgG (3 μg·mL^{-1}). Sections were mounted in FluorSave Reagent (Merck). Signals were visualized and captured by using a fluorescence microscope (model BX50; Olympus) at the same exposure setting for each antibody. Fluorescent areas were quantified by using Image-Pro Plus software (Media Cybernetics).

Confocal Microscopy and 3D Image Reconstruction. Cryostat-cut brain sections, 10 μm thick, from 24-mo-old J20 mice were costained with 5D4 (Cy3, red) and anti-laminin antibody (Alexa-488, green). Signals were visualized with a Total Internal Reflection Fluorescence/Confocal Laser Scanning microscope (A1Rsi, Nikon). The Z-step scans were recorded (1 μm per step, 11 steps). The 3D images were reconstructed and analyzed with NIS-Elements Analysis software (Nikon).

Immunoelectron Microscopy. Preembedding immunoelectron microscopy for 5D4-KS was carried out as described previously (18). Additional details are found in *SI Appendix, SI Materials and Methods*.

Preparation and Structural Analysis of KS. Frozen brain tissues (~100 mg) obtained from NDCs and patients with AD were suspended in 2 mL of 0.2 N NaOH and incubated overnight at room temperature. KS was purified by means of DEAE-Sepharose column chromatography. Disaccharide compositions of KS were determined by reversed-phase ion-pair HPLC with post-column fluorescent labeling, as described previously (34).

Behavioral Testing. During the Y-maze test, mice were placed at the end of one arm (arm length, 40 cm) and allowed to freely explore the Y maze. An observer recorded the number and sequence of arm visits in a single continuous 8-min trial. Each arm was labeled with the letter A, B, or C. Alternation was defined as a consecutive entry in three different arms (e.g., A, B, C, B, A, C, A, C, B; counted as four times of spontaneous alternation). The percentage of spontaneous alternation was calculated as follows: percent alternation = [(number of alternations/total number of entries − 2) × 100]. Testing was performed under dim lighting and a controlled sound background. The apparatus was cleaned with 70% ethanol between trials.

Statistical Analysis. Values were analyzed via the unpaired Student's *t* test (Figs. 1, 3, and 5) or one-way analysis of variance with Tukey's test (Fig. 4*A*) or Dunnett's test (Fig. 4*B*), by using Prism software (GraphPad Software). Differences were regarded as significant when $P < 0.05$. All data are means ± SD unless otherwise noted.

ACKNOWLEDGMENTS. We thank Markus Britschgi for helpful suggestions and discussions; Tomomi Hosono-Fukao, Kuniko Takanose, Hitomi Hoshino, Yuki Kameshima, and Tomoya Ozaki for their technical assistance; and Yoshio Hashizume and Takayuki Yamamoto for their support and diagnostic examinations. This work was supported by the Japanese Health and Labor Sciences Research (Comprehensive Research on Aging and Health Grants H19-001 and H22-007 to K.U. and H20-007 to M.M.), by Grants-in-Aid from the Ministry of Education, Science, Sports and Culture (22790303, 24590349, and 15K08265 to K.U., 23110002 to K.K., Japanese Brain Bank Network for Neuroscience Research and Comprehensive Brain Science Network to H.A.), and in part by the Takeda Science Foundation (K.U.) and the Kobayashi International Scholarship Foundation (K.U.).

1. Kleene R, Schachner M (2004) Glycans and neural cell interactions. *Nat Rev Neurosci* 5(3):195–208.
2. Ohtsubo K, Marth JD (2006) Glycosylation in cellular mechanisms of health and disease. *Cell* 126(5):855–867.
3. van Kooyk Y, Rabinovich GA (2008) Protein-glycan interactions in the control of innate and adaptive immune responses. *Nat Immunol* 9(6):593–601.
4. Rosen SD (2004) Ligands for L-selectin: Homing, inflammation, and beyond. *Annu Rev Immunol* 22:129–156.
5. Crocker PR, Paulson JC, Varki A (2007) Siglecs and their roles in the immune system. *Nat Rev Immunol* 7(4):255–266.
6. Ransohoff RM, Perry VH (2009) Microglial physiology: Unique stimuli, specialized responses. *Annu Rev Immunol* 27:119–145.
7. Prinz M, Priller J (2014) Microglia and brain macrophages in the molecular age: From origin to neuropsychiatric disease. *Nat Rev Neurosci* 15(5):300–312.
8. Saijo K, Glass CK (2011) Microglial cell origin and phenotypes in health and disease. *Nat Rev Immunol* 11(11):775–787.
9. Starossom SC, et al. (2012) Galectin-1 deactivates classically activated microglia and protects from inflammation-induced neurodegeneration. *Immunity* 37(2):249–263.
10. Linnartz B, Bodea LG, Neumann H (2012) Microglial carbohydrate-binding receptors for neural repair. *Cell Tissue Res* 349(1):215–227.

11. Funderburgh JL (2002) Keratan sulfate biosynthesis. *IUBMB Life* 54(4):187–194.
12. Uchimura K (2015) Keratan sulfate: Biosynthesis, structures, and biological functions. *Methods Mol Biol* 1229:389–400.
13. Uchimura K, Rosen SD (2006) Sulfated L-selectin ligands as a therapeutic target in chronic inflammation. *Trends Immunol* 27(12):559–565.
14. Jones LL, Tuszynski MH (2002) Spinal cord injury elicits expression of keratan sulfate proteoglycans by macrophages, reactive microglia, and oligodendrocyte progenitors. *J Neurosci* 22(11):4611–4624.
15. Jander S, Schroeter M, Fischer J, Stoll G (2000) Differential regulation of microglial keratan sulfate immunoreactivity by proinflammatory cytokines and colony-stimulating factors. *Glia* 30(4):401–410.
16. Uchimura K, et al. (2005) A major class of L-selectin ligands is eliminated in mice deficient in two sulfotransferases expressed in high endothelial venules. *Nat Immunol* 6(11):1105–1113.
17. Uchimura K, et al. (1998) Molecular cloning and characterization of an N-acetylglucosamine-6-O-sulfotransferase. *J Biol Chem* 273(35):22577–22583.
18. Foyez T, et al. (2015) Microglial keratan sulfate epitope elicits in central nervous tissues of transgenic model mice and patients with amyotrophic lateral sclerosis. *Am J Pathol* 185(11):3053–3065.
19. Caterson B, Christner JE, Baker JR (1983) Identification of a monoclonal antibody that specifically recognizes corneal and skeletal keratan sulfate. Monoclonal antibodies to cartilage proteoglycan. *J Biol Chem* 258(14):8848–8854.
20. Mucke L, Selkoe DJ (2012) Neurotoxicity of amyloid β-protein: Synaptic and network dysfunction. *Cold Spring Harb Perspect Med* 2(7):a006338.
21. Wyss-Coray T (2006) Inflammation in Alzheimer disease: Driving force, bystander or beneficial response? *Nat Med* 12(9):1005–1015.
22. Meyer-Luehmann M, Prinz M (2015) Myeloid cells in Alzheimer's disease: Culprits, victims or innocent bystanders? *Trends Neurosci* 38(10):659–668.
23. Heneka MT, et al. (2015) Neuroinflammation in Alzheimer's disease. *Lancet Neurol* 14(4):388–405.
24. Mucke L, et al. (2000) High-level neuronal expression of abeta 1-42 in wild-type human amyloid protein precursor transgenic mice: Synaptotoxicity without plaque formation. *J Neurosci* 20(11):4050–4058.
25. Hirano K, et al. (2013) Ablation of keratan sulfate accelerates early phase pathogenesis of ALS. *PLoS One* 8(6):e66969.
26. Takahashi K, Rochford CD, Neumann H (2005) Clearance of apoptotic neurons without inflammation by microglial triggering receptor expressed on myeloid cells-2. *J Exp Med* 201(4):647–657.
27. Wang Y, et al. (2015) TREM2 lipid sensing sustains the microglial response in an Alzheimer's disease model. *Cell* 160(6):1061–1071.
28. Jay TR, et al. (2015) TREM2 deficiency eliminates TREM2+ inflammatory macrophages and ameliorates pathology in Alzheimer's disease mouse models. *J Exp Med* 212(3): 287–295.
29. Prinz M, Priller J, Sisodia SS, Ransohoff RM (2011) Heterogeneity of CNS myeloid cells and their roles in neurodegeneration. *Nat Neurosci* 14(10):1227–1235.
30. Lee S, et al. (2010) CX3CR1 deficiency alters microglial activation and reduces beta-amyloid deposition in two Alzheimer's disease mouse models. *Am J Pathol* 177(5): 2549–2562.
31. Liu Z, Condello C, Schain A, Harb R, Grutzendler J (2010) CX3CR1 in microglia regulates brain amyloid deposition through selective protofibrillar amyloid-β phagocytosis. *J Neurosci* 30(50):17091–17101.
32. Glass CK, Saijo K, Winner B, Marchetto MC, Gage FH (2010) Mechanisms underlying inflammation in neurodegeneration. *Cell* 140(6):918–934.
33. Nishitsuji K, Hosono T, Nakamura T, Bu G, Michikawa M (2011) Apolipoprotein E regulates the integrity of tight junctions in an isoform-dependent manner in an in vitro blood-brain barrier model. *J Biol Chem* 286(20):17536–17542.
34. Hoshino H, et al. (2014) KSGal6ST is essential for the 6-sulfation of galactose within keratan sulfate in early postnatal brain. *J Histochem Cytochem* 62(2):145–156.
35. Lindahl B, Eriksson L, Spillmann D, Caterson B, Lindahl U (1996) Selective loss of cerebral keratan sulfate in Alzheimer's disease. *J Biol Chem* 271(29):16991–16994.
36. Hosono-Fukao T, et al. (2012) Heparan sulfate subdomains that are degraded by Sulf accumulate in cerebral amyloid ß plaques of Alzheimer's disease: Evidence from mouse models and patients. *Am J Pathol* 180(5):2056–2067.
37. Macauley MS, Crocker PR, Paulson JC (2014) Siglec-mediated regulation of immune cell function in disease. *Nat Rev Immunol* 14(10):653–666.
38. Tateno H, Crocker PR, Paulson JC (2005) Mouse Siglec-F and human Siglec-8 are functionally convergent paralogs that are selectively expressed on eosinophils and recognize 6′-sulfo-sialyl Lewis X as a preferred glycan ligand. *Glycobiology* 15(11): 1125–1135.
39. Campanero-Rhodes MA, et al. (2006) Carbohydrate microarrays reveal sulphation as a modulator of siglec binding. *Biochem Biophys Res Commun* 344(4):1141–1146.
40. Patnode ML, et al. (2013) Galactose 6-O-sulfotransferases are not required for the generation of Siglec-F ligands in leukocytes or lung tissue. *J Biol Chem* 288(37): 26533–26545.
41. Linnartz-Gerlach B, Kopatz J, Neumann H (2014) Siglec functions of microglia. *Glycobiology* 24(9):794–799.
42. Griciuc A, et al. (2013) Alzheimer's disease risk gene CD33 inhibits microglial uptake of amyloid beta. *Neuron* 78(4):631–643.
43. El Khoury J, et al. (2007) Ccr2 deficiency impairs microglial accumulation and accelerates progression of Alzheimer-like disease. *Nat Med* 13(4):432–438.
44. Wang Y, et al. (2016) TREM2-mediated early microglial response limits diffusion and toxicity of amyloid plaques. *J Exp Med* 213(5):667–675.
45. Colonna M, Wang Y (2016) TREM2 variants: New keys to decipher Alzheimer disease pathogenesis. *Nat Rev Neurosci* 17(4):201–207.
46. Prokop S, et al. (2015) Impact of peripheral myeloid cells on amyloid-β pathology in Alzheimer's disease-like mice. *J Exp Med* 212(11):1811–1818.
47. Varvel NH, et al. (2015) Replacement of brain-resident myeloid cells does not alter cerebral amyloid-β deposition in mouse models of Alzheimer's disease. *J Exp Med* 212(11):1803–1809.
48. Chiu IM, et al. (2013) A neurodegeneration-specific gene-expression signature of acutely isolated microglia from an amyotrophic lateral sclerosis mouse model. *Cell Reports* 4(2):385–401.
49. Hsiao K, et al. (1996) Correlative memory deficits, Abeta elevation, and amyloid plaques in transgenic mice. *Science* 274(5284):99–102.
50. Uchimura K, et al. (2004) N-acetylglucosamine 6-O-sulfotransferase-1 regulates expression of L-selectin ligands and lymphocyte homing. *J Biol Chem* 279(33): 35001–35008.
51. Hickman SE, Allison EK, El Khoury J (2008) Microglial dysfunction and defective beta-amyloid clearance pathways in aging Alzheimer's disease mice. *J Neurosci* 28(33): 8354–8360.